Integrated waveguide-coupled terahertz microcavity resonators

Paul A. George,[a] Christina Manolatou, and Farhan Rana
School of Electrical and Computer Engineering, Cornell University, Ithaca, New York 14853, USA

Adam L. Bingham and Daniel R. Grischkowsky
School of Electrical and Computer Engineering, Oklahoma State University, Stillwater, Oklahoma 74078, USA

(Received 30 August 2007; accepted 22 October 2007; published online 9 November 2007)

We demonstrate integrated square terahertz microcavity resonators side coupled to waveguides. We present the microcavity transmission spectra for different resonator sizes and coupling strengths. The measured quality factors due to external coupling and cavity loss are found to be between 40 and 90 and between 30 and 40, respectively, for cavity resonance frequencies between 1.077 and 1.331 THz. © *2007 American Institute of Physics*. [DOI: 10.1063/1.2809608]

Integrated terahertz photonic components are important for performing terahertz spectroscopy of vibrational modes in biological and chemical molecules,[1] realizing lab-on-a-chip detection platforms with high sensitivity,[2–4] and developing compact sources of coherent terahertz radiation.[5,6] Although several types of passive terahertz waveguides and resonators have been experimentally demonstrated,[7–9] they have typically been fabricated using bulk micromachining techniques and are not suitable for on-chip integration. In this letter, we experimentally demonstrate for the first time integrated terahertz air-core metallic square microcavity resonators side coupled to metal waveguides. At near-IR wavelengths, evanescent-field coupling is commonly used to excite dielectric microcavities via waveguides.[10] Here, we demonstrate aperture coupling of air-core resonators to waveguides at terahertz frequencies. Strong field enhancement in air-core microcavity resonators can be used for narrowband sensing and the study of terahertz nonlinearities. We present measurements of the cavity quality factors resulting from external coupling and intrinsic cavity loss for different resonator sizes and find good agreement with calculations.

Figure 1 shows a schematic of a square terahertz microcavity resonator, with side d, coupled to a waveguide via an aperture with width w and thickness t. The $\hat{y}$-polarized electric field propagates in the TE_{10} waveguide mode and excites the fundamental TE_{101} mode of the microcavity. Because the spatial profiles of the TE_{10} and TE_{101} modes are constant in the $\hat{y}$ direction, the electromagnetic fields in these modes can be simulated using a two-dimensional finite-difference time-domain (2D-FDTD) method. The simulated resonant terahertz electric field in the structure is shown in Fig. 1.

The terahertz resonators and waveguides under test were fabricated from highly doped 3 in. Si wafers ($N_A = 10^{20}$ cm^{-3}) to avoid measuring terahertz radiation coupled to the substrate. First, one wafer was patterned and etched 150 μm in an inductively coupled plasma deep-Si etcher. The 150 μm etch depth established the waveguide, resonator, and aperture height (dimension in the $\hat{y}$ direction). A scanning electron microscopy (SEM) image of a typical etched structure is shown in Fig. 2(a). As can be seen, the coupling aperture was etched anisotropically and was undercut by 20 μm. Next, both the etched and blank Si wafers were oxidized with 750 nm of thermal oxide. After oxidation, 50 nm of Ti and 400 nm of Au were uniformly deposited on the wafers using an e-beam evaporator with planetary rotation. The thickness of the Au layer was chosen to be greater than five electromagnetic skin depths (~80 nm) at terahertz frequencies.[11] Following evaporation, both wafers were pressed together to form a temporary bond. The wafer stack was then permanently bonded under vacuum on a wafer bonder at a temperature of 350 °C and a pressure of 1.5 MPa for 45 min.[12] Finally, the completed devices were diced to 7 mm long and the facets were polished until optically smooth at terahertz frequencies. Figure 2(b) displays one facet of an air-core rectangular metal waveguide.

Terahertz measurements of the waveguides were conducted using a purged terahertz TD spectrometer (TDS) with a semi-insulating–GaAs photoconductive transmitter and a silicon on sapphire photoconductive receiver.[9] The spectrometer was pumped by an ultrafast Ti:sapphire laser and the power incident upon both the transmitter and receiver was 10 mW. With a lock-in amplifier time constant of 100 ms, the power spectral dynamic range of the experiments was 10^6. Terahertz radiation from the terahertz TDS was coupled into the devices using Si hyperhemispherical lenses butt coupled to each waveguide facet. Multiple scans of each device were performed to ensure the repeatability of spectral features resulting from the excitation of a microcavity.

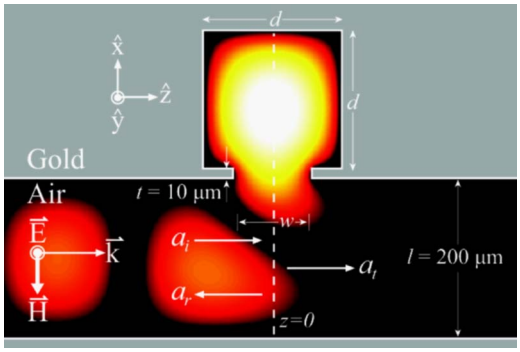

FIG. 1. (Color online) Schematic of a terahertz microcavity resonator side coupled to a metal waveguide overlayed with the simulated terahertz electric field from 2D-FDTD. The square resonator has side d and the coupling aperture has width w and thickness t. The terahertz electric field is polarized in $\hat{y}$ direction and the waveguide is 200 μm wide.

[a]Electronic mail: pag25@cornell.edu

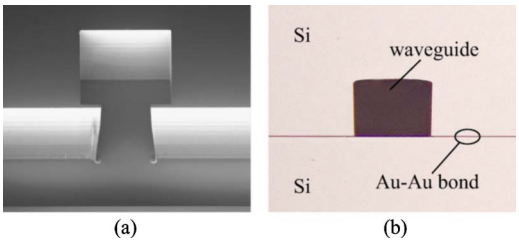

FIG. 2. (Color online) (a) SEM of a fabricated terahertz resonator under test. (b) Photograph of a polished waveguide facet which shows an air-core metal waveguide and Au–Au bond.

Three square resonators with sides $d=175$, 150, and 125 μm coupled to 200 μm wide waveguides via apertures of average widths $w=110$ and 100 μm and thickness $t=10$ μm were measured using the terahertz TDS. As an example, the time-domain terahertz electric field after propagation through a waveguide coupled to a resonator ($d=125$ μm and $w=100$ μm) is shown in Fig. 3. Ringing in the waveform due to waveguide dispersion as well as the frequency-dependent transmission of the resonator extend past 60 ps. Figure 3 also displays the measured power transmitted through the device. The transmission spectrum exhibits a narrow feature at 1.331 THz that corresponds to excitation of the resonant cavity. The strong oscillations in the spectrum that begin at 2.15 THz are characteristic of significant excitation of higher order waveguide modes.[7]

Near the resonant frequency, the evolution of the electric field b inside of a resonator coupled to a single-mode waveguide can be described by coupled mode theory,[13]

$$\frac{db}{dt} = \left(j - \frac{1}{2Q_L} - \frac{1}{2Q_E}\right)\omega_0 b + \sqrt{\frac{\omega_0}{2Q_E}}a_i. \quad (1)$$

In Eq. (1), ω_0 is the resonance frequency, Q_E and Q_L are the cavity quality factors related to external coupling and intrinsic cavity loss, respectively, and a_i is the incident waveguide field (Fig. 1) normalized such that its squared magnitude equals the incident power. The transmitted field is a_t, where $a_t=a_i-b\sqrt{\omega_0/2Q_E}$.[13] After combining this equation with the time-harmonic solution to Eq. (1), the expression obtained

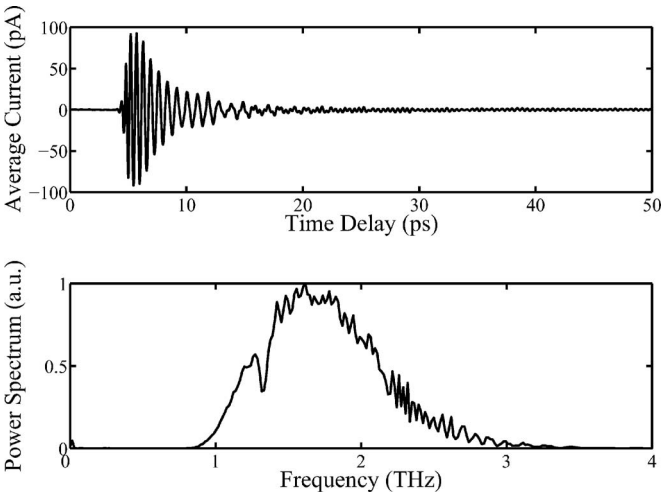

FIG. 3. Measured terahertz time-domain electric field waveform and accompanying power spectrum after propagation through a resonator structure ($d=125$ μm and $w=100$ μm). The resonance dip at 1.331 THz is evidence of excitation of the resonator mode.

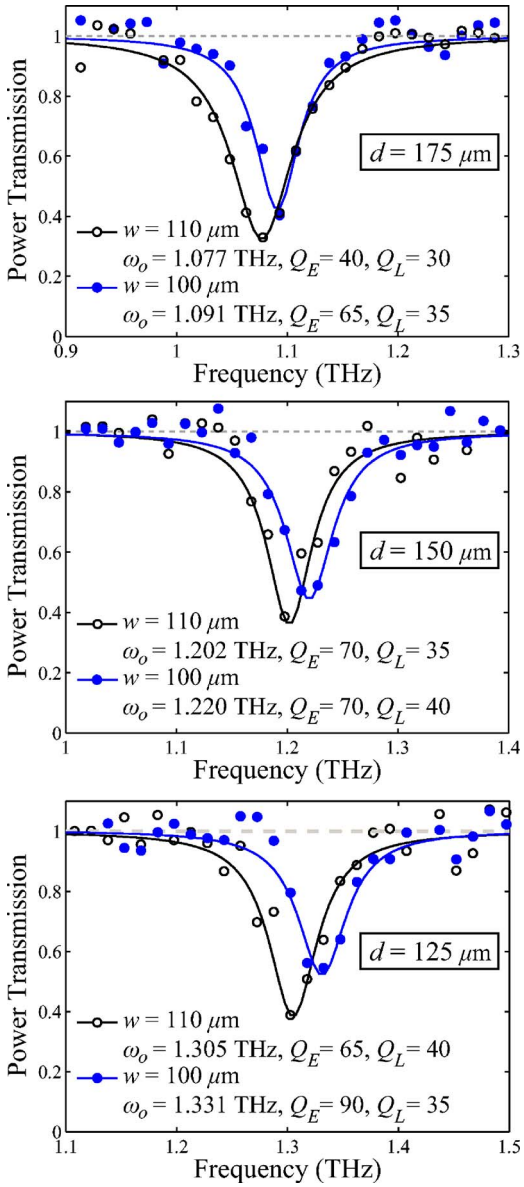

FIG. 4. (Color online) Microcavity transmission spectra for resonators with $d=175$, 150, and 125 μm and average $w=110$ and 100 μm. Measured values Q_E are between 40 and 90 and a data extraction error of less than 10% is expected.

for the frequency-dependent power transmission of the coupled waveguide-resonator system $T(\omega)$ is

$$T(\omega) = \left|\frac{a_t}{a_i}\right|^2 = \left|1 - \frac{1/Q_E}{1/Q_E + 1/Q_L - 2j(1-\omega/\omega_0)}\right|^2. \quad (2)$$

This expression has a Lorentzian shape and is applicable for frequencies close to ω_0. From Eq. (2), it can be seen that the power transmission at resonance is reduced from unity and is exactly zero for lossless cavities ($Q_L=\infty$). This occurs because the electromagnetic radiation coupled from a lossless resonator back into the waveguide in the forward direction interferes completely destructively with the incident radiation a_i.

As shown in Fig. 4, the microcavities affect the measured terahertz TDS spectra only in a narrow frequency range near resonance. To extract the microcavity transmission spectra, the measured terahertz TDS spectra with resonances removed were fitted with fifth-order polynomials near

TABLE I. Measured and simulated values of ω_0, Q_E, and Q_L for $d=175$ μm. Good agreement exists between the experimental and 2D-FDTD results for ω_0 and Q_E. Large discrepancy in Q_L may be due to imperfect metallization and defects in the Au–Au bond.

d (μm)	w (μm)	ω_0 (THz)	Q_E	Q_L
		Measured		
175	110	1.077	40	30
175	100	1.091	65	35
		2D-FDTD		
175	110	1.117	55	370
175	100	1.132	80	354

the resonance frequencies and the total terahertz TDS spectra were then normalized with these polynomials. Figure 4 shows the transmission spectra of different cavities obtained in this way. The Lorentzian expression in Eq. (2) was fitted to the measured microcavity transmission spectra to obtain the values of ω_0, Q_E, and Q_L, which are also shown in Fig. 4. It can be seen that the measured transmission spectra are well described by a Lorentzian near the resonance frequency. The values of Q_E and Q_L changed by less than 10% when a third-order polynomial was used to extract the transmission spectra.

The increase of ω_0 and Q_E with decrease in w matches closely the trends predicted by 2D-FDTD simulations. Table I shows the measured data and simulated results obtained from 2D-FDTD for $d=175$ μm and w averaged to account for the 20 μm etch undercut mentioned previously. The small discrepancies between these measured and FDTD values can be attributed to nonidealities in the structure dimensions and sidewall verticality that cannot be modeled by two-dimensional simulations. Similar agreement exists between FDTD results and experimental data for the other resonators shown in Fig. 4 ($d=150$ and 125 μm).

As can be seen in Table I, the measured and simulated values of Q_L differ significantly. Using a conductivity of 38×10^6 S/m for Au at 1 THz,[11,14] the calculated values of Q_L are between 291 and 370 for all the cavity geometries studied in this work. These values are significantly larger than the measured values of 30–40 presented in Fig. 4. This disagreement may partially be due to the reduced conductivity of evaporated Au at terahertz frequencies[15] but is more likely attributable to defects in the Au–Au bond. Imperfections in the bond could lead to a contact resistance of several ohms that would add in series with the resistance due to Ohmic losses in the cavity sidewalls (~0.4 Ω). The calculated values of Q_L agree well with the measured values if a bond resistance of ~3 Ω is assumed.

In conclusion, we have demonstrated integrated terahertz microcavity resonators side coupled to metal waveguides. The extracted values of Q_E for these devices are between 40 and 90 and agree well with results from 2D-FDTD. However, the measured values of Q_L are much smaller than those predicted by simulations. From Eq. (1), the estimated enhancement of the square magnitude of the peak terahertz electric field in the microcavity resonator to that in the waveguide is between 8 and 18 for all of the structures in this work. Achieving strong field enhancement in integrated structures would, therefore, require terahertz microcavities with small intrinsic cavity losses. Such structures would be well suited for narrowband sensing applications, developing integrated sources of terahertz radiation, and studying THz nonlinearities.

This work was supported by the National Science Foundation.

[1] D. L. Woolard, W. R. Loerep, and M. S. Shur, *Terahertz Sensing Technology* (World Scientific, New Jersey, 2003), Vols. 1 and 2, p. 1.
[2] J. S. Melinger, N. Laman, and S. S. Harsha, and D. Grischkowsky, Appl. Phys. Lett. **89**, 251110 (2006).
[3] M. Nagel, P. H. Bolívar, M. Bruscherseifer, H. Kurz, A. Bosserhoff, and R. Büttner, Appl. Opt. **41**, 2074 (2002).
[4] H. Kurt and D. S. Citrin, Appl. Phys. Lett. **87**, 041108 (2005).
[5] G. Fasching, A. Benz, K. Unterrainer, R. Zobl, A. M. Andrews, T. Roch, W. Schrenk, and G. Strasser, Appl. Phys. Lett. **87**, 211112 (2005).
[6] P. A. George, C. Manolatou, F. Rana, and A. I. Akinwande, Proceedings of the 2005 Conference on Lasers and Electro-Optics, 2005 (unpublished). Paper no. CThX5.
[7] G. Gallot, S. P. Jamison, R. W. McGowan, and D. Grischkowsky, J. Opt. Soc. Am. B **17**, 851 (2000).
[8] K. Wang and D. M. Mittleman, Nature (London) **432**, 376 (2004).
[9] A. L. Bingham and D. Grischkowsky, Appl. Phys. Lett. **90**, 091105 (2007).
[10] K. Vahala, *Optical Microcavities* (World Scientific, New Jersey, 2004), Vol. 5, p. 9.
[11] D. M. Pozar, *Microwave Engineering*, 3rd ed. (Wiley, New Jersey, 2005), p. 687.
[12] C. H. Tsau, S. M. Spearing, and M. A. Schmidt, J. Microelectromech. Syst. **11**, 641 (2002).
[13] C. Manolatou, M. J. Khan, S. Fan, P. R. Villeneuve, H. A. Haus, and J. Joannopoulos, IEEE J. Quantum Electron. **35**, 1322 (1999).
[14] B. Williams, H. Callebaut, S. Kumar, and Q. Hu, Appl. Phys. Lett. **82**, 1015 (2003).
[15] N. Laman and D. Grischkowsky, Appl. Phys. Lett. **90**, 122115 (2007).